Chiang Mai J. Sci. 2018; 45(5) : 2034-2047
http://epg.science.cmu.ac.th/ejournal/
Contributed Paper

Microstructure and Wear Behavior of Hardfacing with Ferro-alloy Powder Addition Using Submerged Arc Welding

Buntoeng Srikarun and Prapas Muangjunburee*
Department of Mining and Materials Engineering, Faculty of Engineering, Prince of Songkla University, Hat Yai, Songkhla, 90112 Thailand.
* Author for correspondence; e-mail: prapas.m@psu.ac.th

Received: 1 November 2017
Accepted: 30 April 2018

ABSTRACT

Hardfacing deposits with the additional metal powder become an intense development in the wear resistant applications. Low carbon steel electrode with carbon and chromium powder addition is used to improve the wear resistance of engineering components due to its martensite microstructure. The objectives of this research are to investigate the effect of ferro carbon, ferro chromium, and the mixture of ferro carbon and ferro chromium powder addition to the low carbon steel electrode deposits and compared to the standard martensitic steel type electrode without powder addition. Low alloy cast steel was hardfaced by submerged arc welding (SAW) process. The chemical composition of the weld metal for all conditions was studied using Optical Emission Spectrometer (OES) and Energy Dispersive X-ray Spectroscopy (EDS). Optical Microscope (OM), Scanning Electron Microscope (SEM) and X-Ray Diffraction (XRD) were used to analyze the metallurgical properties of the samples. Vickers hardness test and a dry sand rubber wheel abrasion test were also conducted. The results showed that the martensite microstructure varied with the welding conditions. The best abrasive wear resistance was obtained in the microstructure composed of a large martensite with dendritic ferrite, while the higher abrasive mass loss was measured in the microstructure of martensite with retained austenite. The main wear mechanisms observed at the worn surfaces included micro-cutting and micro-ploughing of the soft matrix and brittle fracture of the martensite structure.

Keywords: hardfacing, submerged arc welding, microstructure, hardness, Aabrasive wear resistance

1. INTRODUCTION

Hardfaced coatings are the best way to improve the service life of machine components under severe duty [1-2]. Hardfacing is applied to both new and old component where the components are easy to wear. The high alloy hardfacing materials offer much better wear resistance than the original base material [3]. This material usually

increases the service life of the components up to two or more times compared with components without hardfacing [4]. In the hardfacing technologies, high carbon and chromium alloys steel are widely used in mining and processing industry because of a large fraction of carbides in microstructure [5-6]. High carbon and chromium hardfacing showed the large area of brittle carbides, which were easy to crack. Therefore, these alloys have some limitation to use in the wear-related operation, especially for the impact wear [7].

The martensitic hardfacing electrode is one of most useful hardfacing materials submitted to severe wear conditions [8-9]. For the time being, martensitic steel electrode is very suitable materials for the hardfacing procedure to repair the single roll coal crusher in Electricity Generating Authority of Thailand (EGAT), Mae Moh Mine because it has enough hardness and toughness to resist a combination of abrasion and impact wear. The weld hardfacing with additional metal powder is a new hardfacing technique to reduce the high cost of the electrode. Powder addition in the welding procedures has been used in various branches of mining industry [10-11].

Several welding processes such as shielded metal arc welding (SMAW), Gas metal arc welding (GMAW), flux core arc welding (FCAW) and submerged arc welding (SAW) are used to deposit the hardfacing. The most significant factors to select welding process are the welding efficiency and cost of consumables. [12-13] The most desirable process for hardfacing and fabrication in the industry is submerged arc welding process because it offers several advantages such as being able to use multiple-electrodes at the same time and powder addition, easier automatic application, lower welder skill requirement, high deposition rate and safe operation environment [14-15].

Most researchers discussed that the martensite microstructure can increase hardness and wear resistance of hardfacing deposits, as well as a lot of papers, have been published their results on wear resistance of martensitic hardfacing obtained using a variety of different hardfacing processes. However, there are very few studies concerning the wear behavior of ferrocarbon and ferrochromium powder addition to producing martensitic structure of hardfacing using submerged arc welding process. Therefore, in this study, the wear behavior of metal powder addition to increasing martensitic structure of hardfacing was investigated and compared with hardfacing using standard martensitic steel electrode without powder addition. Macro/microstructure, chemical composition, spectra of X-ray diffraction analysis, and mechanical properties consist of hardness and abrasive wear resistance were investigated.

2. MATERIALS AND METHODS

2.1 Materials and Welding Procedures

In this research, the size of low chromium alloy steel (3.5% Cr steel) plates were cut to 75 mm × 250 mm × 20 mm for the base metal. The hardfaced deposit using AC/DC inverter power source Esab Aristo 1000 AC/DC SAW with the universal welding automat Esab A2 Multitrac A2TF twin-wire submerged arc welding process. The chemical composition of the base metal shows in Table 1. Preheating temperature of 3.5 % Cr steel were maintained at 350 °C and it depended on carbon equivalent value of 1.247 % according to equation (1) [16]. For the first step of welding procedures, buffer layer electrode (EN 14700: T Fe10) was directly deposited onto the 3.5 % Cr steel plate. After depositing the single buffer layer three hardfacing layers were applied

over the single buffer layer, see in Figure 1. Four samples were welded using different hardfacing materials. These samples named Ms, Fe-Cr, Fe-C, and Fe-C-Cr. Martensitic steel electrode (EN 14700: T Fe 8) without powder addition was used to weld for the Ms sample. Low carbon steel electrode (EN 756 S2Si) with ferro chromium powder addition was welded for the Fe-Cr sample. The Fe-C sample was hardfaced using low carbon steel electrode with ferro carbon powder addition. The last sample, Fe-C-Cr was deposited by low carbon electrode with the combination of ferro carbon and ferro chromium powder addition. To obtain the considerable hardfacing deposits, the powder was placed on top of the welded layer along the travel of welding head. The thickness of the additional powder to deposit weld metal are different. For the Fe-Cr sample is 1.5-2.0 mm, Fe-C sample is 3-4 mm and the Fe-C-Cr sample is 5-6 mm. The flux for submerged arc welding was employed high basics flux. Chemical compositions of buffer electrode, martensitic electrode, low carbon steel electrode, additional powder and flux from manufacturer data sheets are given in Table 2 and 3. In this experiment, the Ms sample was represented as the targeted conditions in terms of chemical composition. Therefore, the amount of additional powder is calculated by referring to the alloying contents of Ms sample. The different welding conditions and the detail of welding parameters are provided in Table 4 and 5.

$$\text{Carbon Equivalent (CE)} = \text{C} + \frac{1}{6}\text{Mn} + \frac{1}{24}\text{Si} + \frac{1}{40}\text{Ni} + \frac{1}{5}\text{Cr} + \frac{1}{4}\text{Mo} + \frac{1}{14}\text{V}(\%) \quad (1)$$

Table 1. Chemical composition of 3.5 % Cr steel for base metal (wt. %).

C	Si	Mn	Ni	Cr	Mo	Fe
0.38	0.40	0.52	0.17	3.42	0.30	Balance

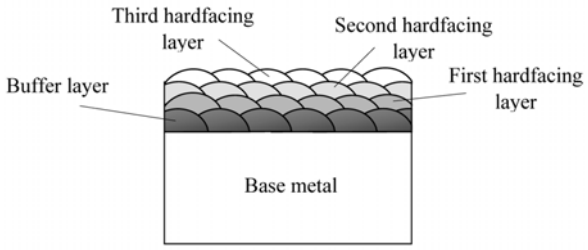

Figure 1. Schematic diagram of welding layers.

Table 2. Chemical composition of electrodes and additional powder (wt. %).

Materials	C	Mn	Si	Cr	Ni	Fe
EN 14700: T Fe10	0.10	6.00	0.50	19.0	9.0	Balance
EN 14700: T Fe 8	0.50	1.50	2.50	8.50	-	Balance
EN 756 S2Si	0.10	1.00	0.20	-	-	Balance
Ferro chromium powder	0.04	-	2.90	34.7	0.43	Balance
Ferro carbon powder	1.2	-	0.05	-	-	Balance

Table 3. Chemical composition of agglomerated flux (wt. %).

$SiO_2 + TiO_2$	CaO + MgO	$Al_2O_3 + MnO$	CaF_2
18	35	23	22

Table 4. Welding conditions used during hardfacing.

Sample	Materials			
	Martensitic electrode (g/cm)	Low carbon electrode (g/cm)	Ferro chromium powder (g/cm)	Ferro carbon powder (g/cm)
Ms	2.0	-	-	-
Fe-Cr	-	2.0	0.6	-
Fe-C	-	2.0	-	1.6
Fe-C-Cr	-	2.0	2.4	1.2

Table 5. Twin-wire submerged arc welding for hardfacing deposits.

Fixed parameter	Value
Current (A)	600
Voltage (V)	30
Polarity	DC+
Electrode diameter (mm)	2.4
Electrode extension (mm)	25
Welding speed (cm/min)	60
Heat input (kJ/cm)	18.0

2.2 Characterization

Chemical analysis, macro/microstructural characterization, hardness test and wear test were conducted on the third hardfacing layer. The only reason why the third layer is selected to analyze is to avoid the dilution effect with the buffer layer. The chemical composition was determined by Thermo ARL 3460 optical emission spectrometry (OES) on the top surface of the samples. The macro/microstructure of transverse cross-section was characterized by Carl Zeiss Axio Scope.A optical microscope (OM). Oxford energy-dispersive x-ray spectroscopy (EDX) was used to qualitatively describe chemical variation in the microstructure. The specimens for metallographic investigation were polished and etched with Viella's reagent (5 ml HCl, 2 g picric acid, 100 ml methyl alcohol). Philips X' Pert MPD x-ray diffraction (XRD) of hardfaced coating were carried out on the grinded top surface layer.

2.3 Mechanical Testing

According to ASTM E 384-11e1 [17], hardness values were measured by Matsuzawa MMT-X7B micro hardness testing under 1,000 gf and 200 gf loads of dwell time for 10 seconds. Micro hardness values of different area were measured across the cross-section of welding sample from the base metal to third hardfaced layer. Furthermore, micro hardness values were randomly taken ten points on the top surface of hardfacing layers.

A dry sand rubber wheel abrasive wear test machine according to ASTM G 65-00e1 [18] was run to investigate wear resistance of the hardfaced layers. The schematic diagram of dry sand abrasion machine is shown in Figure 2. Abrasion test samples were cut to 25.4 mm × 75 mm × 12.7 mm dimension and grinded the surface. SiO_2 natural sands (212 and 300 μm) was used as abrasive particles, which was baked at 150 °C inside the furnace for 1 hr and then

cooled to room temperature before running the test. Parameters of wear test are given in Table 6. Mass loss data was recorded by Denver TB-214 instrument for all samples. The abrasive wear resistance was calculated as shown in equation (2) [19]. The wear mechanisms and conditions of worn surfaces were examined by FEI Quanta 400 scanning electron microscope (SEM) equipped with secondary electron detector.

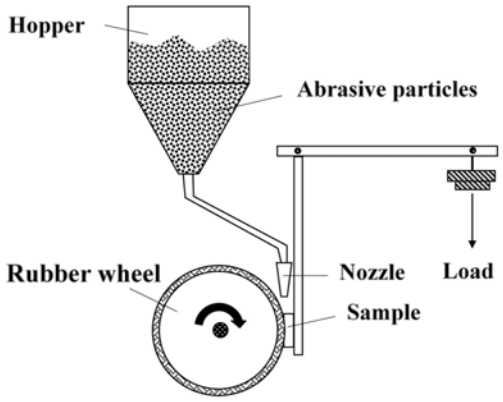

Figure 2. Schematic diagram of abrasion testing machine according to ASTM G 65.

$$\text{Abrasive wear resistance} = \frac{\text{Wear distance (m)}}{\text{Mass loss (mg)}} \quad (2)$$

Table 6. Wear testing parameters.

Parameter	Value
Procedure	A
Load (N)	130
Velocity (rpm)	200
Sand flow rate (g/min)	250
Wear distance (m)	4309

3. RESULTS AND DISCUSSION

3.1 Macrostructure

The macrostructure of each hardfacing deposit consist of one buffer layer and three hardfacing layers welded with four different hardfacing materials are shown in Figure 3. The area of heat affected zone and the buffer layer in the macrographs showed no cark and other welding defects. According to the macrostructural results, the Ms sample has a thickness of hardfaced layer approximately 2-3 mm. The thickness of the hardfaced samples with powder addition are also different. The Fe-Cr sample showed about 3-4 mm, Fe-C sample showed about 4-5 mm and then Fe-C-Cr sample showed about 4-6 mm. The sample welded with only martensitic (Ms) steel electrode showed lower thickness of hardfaced deposits than the samples welded with low carbon steel with powder addition (Fe-Cr, Fe-C and Fe-C-Cr) because the sample welded without powder addition using same heat input as the powder addition sample needed to melt only electrode into weld pool, while the samples welded with powder addition needed to melt both electrode and additional powder into weld pool. Therefore, powder addition can increase the deposition rate and decrease level of dilution in the weld metal. The percent dilution of Ms sample is about 56% while the percent dilution of the sample Fe-Cr, Fe-C and Fe-C-Cr are about 43%, 33%, and 21% respectively. Welding defects such as macro cracks, porosities, and clusters of particles can be seen in Figure 3 (c) and (d). The particle clusters in hardfaced deposits occurred due to undissolved powder and the cracks were growing through these clusters because of the residual stresses [20]. The formation of porosities in welded metal was also described that it was the entrapped bubbles inside the powder.

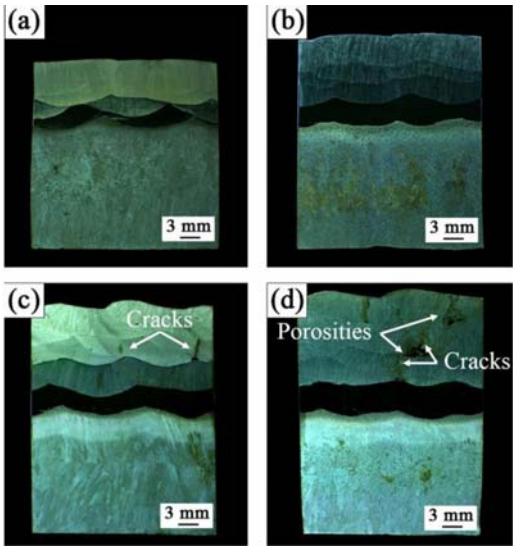

Figure 3. Macrostructure of the cross-sectional welding samples (a) Ms sample (b) Fe-Cr sample (c) Fe-C sample (d) Fe-C-Cr sample.

3.2 Chemical Composition

The chemical composition of each hardfacing deposit shows in Table 7 and it presents considerable variation among the deposits. The chemical composition of sample welded with martensitic steel electrode showed the highest content of chromium, manganese, and nickel, but carbon content is approximately similar to the sample welded using the combination of ferro carbon and ferro chromium powder addition. This composition produced the microstructure of martensite with retained austenite and resisted the abrasive wear. The additional metal powder increased the specific elements in the chemical composition. When the Fe-Cr sample was welded, low carbon steel electrode and additional ferro chromium powder were melted into the weld pool. This sample showed high chromium content in the weld metal. The other metal powder addition sample also increased the chemical elements in the welded samples. Carbon content increased in the Fe-C sample and carbon and chromium content increased in the Fe-C-Cr sample. The chemical composition of Ms sample was noticed as the standard. Therefore, the additional metal powder in the hardfacing layers was applied in order to get sufficient amount of carbon and chromium in the weld sample metal like the Ms sample using the standard martensitic steel electrode. Carbon and chromium played the major elements to appear martensitic structure.

Table 7. Chemical composition of the third hardfacing layer by optical emission spectroscopy (wt. %).

Sample	C	Si	Mn	Ni	Cr	Mo	V
Ms	0.44	1.12	2.24	1.02	9.09	0.42	0.30
Fe-Cr	0.12	1.08	1.21	0.76	8.75	0.03	0.02
Fe-C	0.34	0.27	0.94	0.25	0.82	0.02	0.01
Fe-C-Cr	0.47	0.76	0.66	0.14	7.60	0.02	0.02

3.3 Microstructure

Figure 4 and 5 show the microstructure and energy dispersive X-ray spectra obtained from the cross-section of third hardfacing for four different conditions. The microstructure of the sample welded with martensitic steel is shown in Figure 4 (a). This figure presents a mixture of needle-shaped martensite (dark region) and retained austenite (white region) in the grain boundaries with a refined pattern of dendritic segregation [21]. EDX spectrum for the Ms sample is depicted in Figure 5 (a). This result gave the high amount of carbon and chromium content. The retained austenite

phase was formed when austenite could not completely transform to martensite upon the immediate cooling from very high temperature and then the alloying elements of manganese and nickel in the chemical composition of Ms sample are austenite former [22]. Figure 4 (b) shows the microstructure of Fe-Cr deposit. In the microstructure of Fe-Cr sample, white region represents ferrite microstructure and dark region represents martensite microstructure. Increasing chromium content leads to the formation of martensite in this hardfaced layer, the basic reason is that the chromium content in the matrix increases the hardenability of the matrix. High chromium peak in EDX spectrum of the Fe-Cr sample can be seen in Figure 5 (b). The mixture of ferrite and bainite microstructure and EDX spectrum of the Fe-C sample are shown in Figure 4 (c) and Figure 5 (c). In this image, white region represents ferrite phase and dark region represents bainite phase. Ferrite normally shows the welded microstructure of conventional low carbon steel, while bainite structure observed in the weld metal depended on the chemical composition and cooling rate. Carbon prefers to produce bainite in the multi-pass welded microstructure of low carbon steel because these welded deposits experienced a full austenization induced by heat input of welding process, and then these deposits reheated to high temperature when the adjacent layer was welded. It can provide slow cooling rate. The first-step full austenization creates bainite or martensite microstructure. During the second-step reheating temperature reversed austenite preferentially nucleates at the prior austenite grain boundary and transforms to bainite during the cooling process [23]. The formation of bainite strongly resembles that of pearlite, but bainite is formed finer with the cementite stringers more numerous and more continuous. Figure 4 (d) shows the microstructure of the Fe-C-Cr sample, which contains fully martensite structure with dendritic ferrite matrix. Carbon and chromium were the main alloying element for this sample to produce and enlarge martensite structure. The martensite structure of this welding condition expected as a mixed lath and plate martensite. Figure 5 (d) shows the EDX spectra of Fe-C-Cr sample resulted in ferrite and martensite, which is an evident to identify high carbon and chromium of this microstructure.

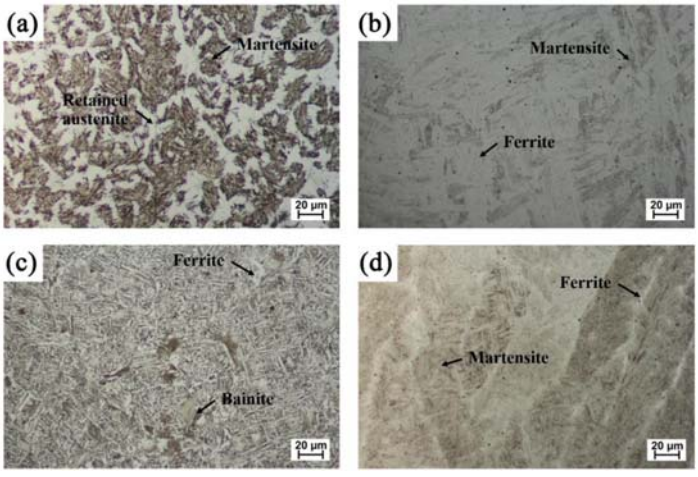

Figure 4. Microstructure of the cross-sectional deposit layer (a) Ms sample (b) Fe-Cr sample (c) Fe-C sample (d) Fe-C-Cr sample.

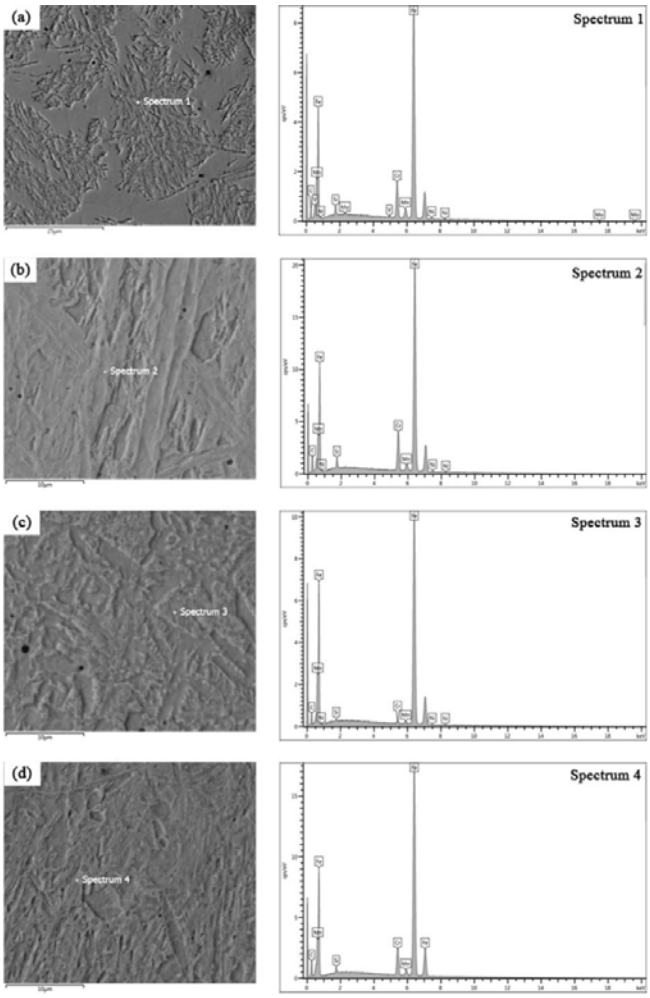

Figure 5. EDX point scan analysis on third hardfacing (a) Martensitic steel (b) low carbon steel with ferro chromium powder (c) low carbon steel with ferro carbon powder (d) low carbon steel with ferro chromium and ferro carbon powder.

Figure 6 illustrates XRD analysis results of hardfacing deposit layers with the different composition. The microstructure of the deposits using martensitic steel electrode without powder addition (Ms) showed martensite and retained austenite [21]. XRD spectra of the Fe-C sample showed strongly consisted of only ferrite peak. [24]. While the peak of ferrite and martensite which were located at the coincident [25] were detected in that of the Fe-Cr sample. The Fe-C-Cr sample used high content of carbon and chromium powder addition showed an over lab of ferrite and martensite peak as well. The austenite microstructure can only be seen in the microstructure of the Ms sample because the alloying element of additional powder contained the lower amount of austenite former elements, such as nickel and manganese.

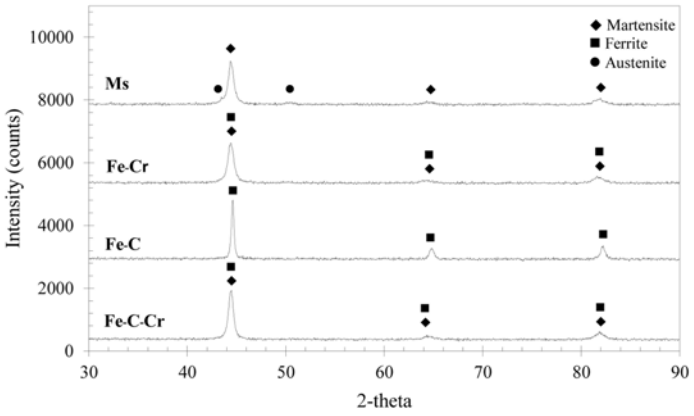

Figure 6. XRD results of samples, Ms: martensite and austenite, Fe-C: Ferrite, Fe-Cr: martensite and ferrite, Fe-C-Cr: martensite and ferrite.

3.4 Hardness

Micro hardness distributions across the base metal (BM), heat affected zone (HAZ), first hardfacing layer (HF 1), second hardfacing layer (HF 2) and third harfacing layer (HF 3) of all welded samples are displayed in Figure 7. Table 8 shows the average hardness values of each zone of cross-sectional welding sample. The average hardness of the base metal showed 190.2 HV. The hardness distribution across heat affected zone were different. The highest hardness in heat affected zone revealed the sample welded without powder addition, whereas the sample welded with the highest content of powder addition presented lowest hardness. Heat input for the welding process had less effect on the heat affected zone when the metal powder was added. It is due to the fact that some heat input is distributed to fusion of the additional metal. The average hardness of buffer layer showed 262.3 HV in accordance with austenitic stainless-steel property. Hardness distribution through hardfaced deposits of the Ms sample is shown in Figure 7(a). For the Ms sample, lower hardness value about 439.3 HV was observed in the first hardfacing layer due to the dilution with the austenitic buffer layer. The average hardness value of the second hardfacing and third hardfacing were nearly identical and these values were about 551.1 HV. There was no dilution with the austenitic buffer layer in these layers. Figure 7(b) presents hardness profiles of Fe-Cr sample. The hardness values about 408.9 HV showed the first to the third hardfacing layer of the Fe-Cr sample. The microstructure of the Fe-Cr sample showed a large area of ferrite matrix mixed with small amount of martensite. Thus, the hardness values of this sample were low. Chromium gives higher hardness because it can combine with other element to form the hard phase like carbide or martensite. Dissolving chromium in ferrite has no limit and it can mainly affect the mechanical properties through solid solution hardening. [26]. Hardness profile of the Fe-C sample can be seen in Figure 7 (c), it presents a high range of the hardness variation in harfacing. In the third hardfacing of Fe-C sample, ferrite and bainite microstructure gave the lowest hardness of 264.9 HV. Figure 8 (d) presents hardness distribution of Fe-C-Cr hardfacing deposits. The highest hardness values of hardfacing layer resulted in about 603.2 HV and correlated with martensite microstructure. The hardness values of the third hardfacing for both the Ms sample and Fe-C-Cr sample were similar.

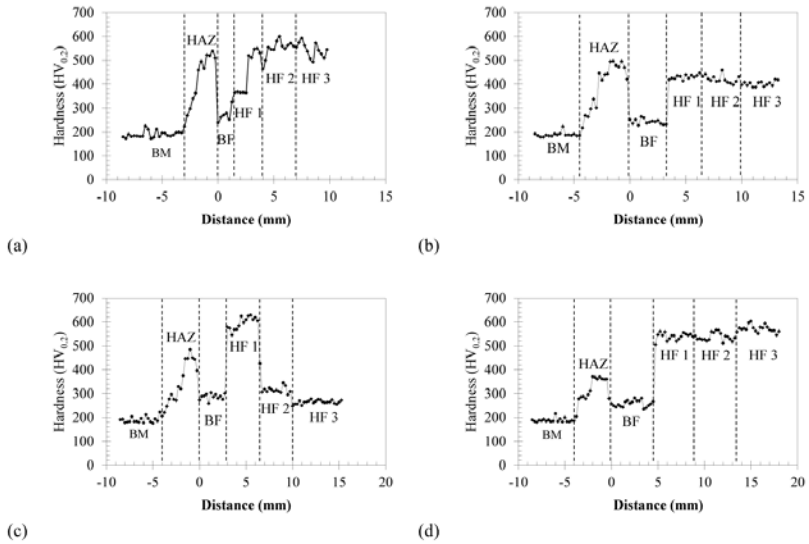

Figure 7. Hardness profiles across the cross-section of samples (a) sample of Ms (b) sample of Fe-Cr (c) sample of Fe-C (d) sample of Fe-C-Cr.

Table 8. Average hardness values of each zone of cross-sectional welding sample.

Sample	Average hardness ($HV_{0.2}$)					
	BM	HAZ	BF	HF 1	HF 2	HF 3
Ms	189.1	416.6	260.2	439.3	556.4	541.7
Fe-Cr	189.4	408.9	243.0	430.5	418.6	401.9
Fe-C	192.7	362.0	285.9	576.6	323.5	264.9
Fe-C-Cr	189.4	330.2	260.0	540.5	537.8	570.2

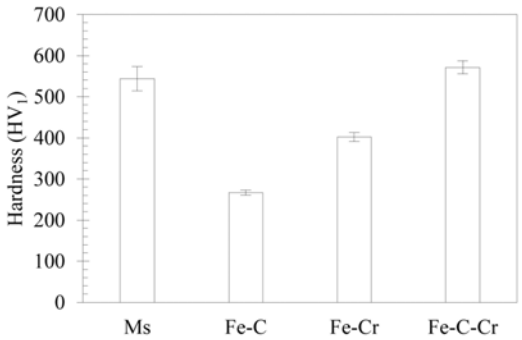

Figure 8. Hardness results from the top surface layer of third hardfacing deposits.

The average micro hardness results taken on the top surface of hardfacing deposit is shown in Figure 8. It can be clear that the different hardfacing materials changed the hardness values of the welded metal significantly. The higher the additional carbon and chromium elements led to the higher the hardness value of hardfacing. The hardfacing deposit of Fe-C-Cr sample showed the highest hardness value, whereas the lowest hardness value was obtained from the Fe-C hardfacing, which contained high carbon content in the weld metal. Fe-Cr hardfacing revealed higher hardness than Fe-C hardfacing because of increasing chromium content of the weld metal, that formed martensite microstructure in the deposit.

3.5 Abrasive Wear Resistance and Worn Surface

The abrasive wear resistance for all conditions is shown in Figure 9. The hardfacing deposits of Ms sample showed lower abrasive wear resistance than that of the sample welded using low carbon steel electrode with metal powder addition. The austenite phase is easy to cut and remove by abrasive particles due to its ductile properties. Therefore, the sample using martensitic steel electrode contained martensite with retained austenite microstructure showed the lower abrasive wear resistance, which was the same result as the previous work [27]. For the powder addition samples, the greater wear resistance was obtained because of their unique combination of different microstructures. Carbon and chromium played a crucial role in the abrasive wear resistance of hardfacing because these elements gave a large amount of martensite with dendritic ferrite microstructure, which served as a barrier against the abrasive particles cutting on the surface. The hardness values on the top surface of all powder addition samples showed a direct correlation with the abrasive wear resistance. The higher hardness gave the superior wear resistance for all powder addition samples.

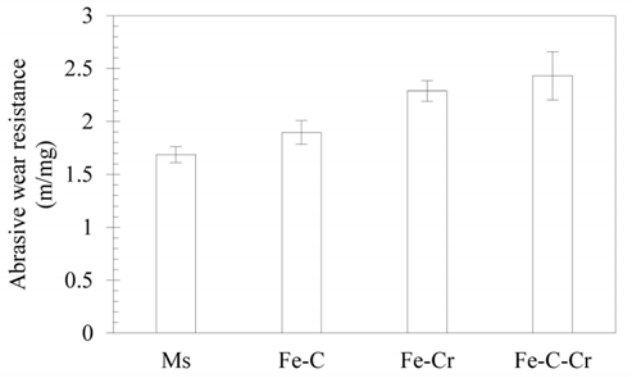

Figure 9. Abrasive wear resistance index for all conditions.

The SEM images of the worn surface are shown in Figure 10. Figure 10 (a) shows the worn surface of the Ms sample. The main mechanism of the worn surface in the Ms sample was micro-cutting and some area of the worn surface showed the deep micro-ploughing grooves. These mechanisms resulted in the lowest wear resistance. Figure 10 (b) and (c) show the worn surface of the Fe-Cr sample and the Fe-C sample. Both samples were worn by micro-cutting and brittle fracture. The Fe-C sample presented the lowest abrasive wear resistance compared to other powder addition sample because its worn surface showed a large area of the brittle fracture. In Figure 10 (d), the worn surface of the Fe-C-Cr samples showed the abrasive mechanism included micro-cutting, micro-ploughing, and brittle fracture. A large horizontal crack can be seen in the SEM image of the Fe-C-Cr sample. This crack was not because of the abrasive wear operation, but because of the welding defect. In addition, the shallow micro-ploughing grooves were observed in this sample. The highest abrasive wear resistance was studied in the Fe-C-Cr sample.

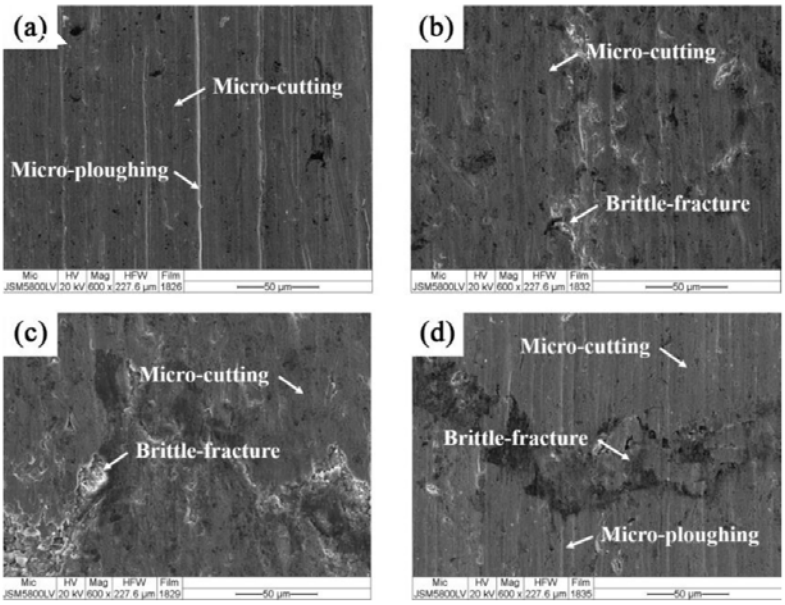

Figure 10. Typical aspect of worn surfaces (a) Ms sample (b) Fe-Cr ample (c) Fe-Cr sample (d) Fe-C-Cr sample.

4. CONCLUSIONS

Hardfacing deposits were produced using submerged arc welding. The influence of metal powder addition on the metallurgical properties and mechanical properties of hardfacing can be summarized as follow:

(1) Hardfacing with powder addition presented higher abrasive wear resistance than hardfacing by the standard martensitic electrode.

(2) Additional ferro carbon and chromium powder produced martensitic and ferritic microstructure with high hardness, resulting in higher wear resistance, while the sample welded using martensitic steel type wire resulted in a high hardness with the martensite and retained austenite microstructure, but its wear resistance was lower.

(3) The Fe-C-Cr sample is the best condition of the present research because this sample shows martensitic and ferritic structure that is highest hardness and wear resistance. The main abrasive wear mechanisms of Fe-C-Cr sample, such as micro-cutting, micro-ploughing and brittle fracture were found on the worn surfaces.

(4) All samples welded with powder addition showed the correlation between the top surface hardness and wear resistance of hardfacing deposit. However, the hardfacing of Ms sample only showed higher top surface hardness with lower wear resistance.

(5) The most important factor for the wear resistance of hardfacing is the microstructure of deposits.

ACKNOWLEDGEMENTS

This research was financially supported by the government budget of Prince of Songkla University, contract ENG600279S. The authors would like to acknowledge the Electricity Generating Authority of Thailand (EGAT), Mae Moh Mine and Department of Mining and Materials Engineering, Faculty of Engineering, Prince of Songkla University, Thailand for providing important information and equipment.

REFERENCES

[1] Lemke J.N., Rovatti L., Colombo M. and Vedani M., *Mater. Des.*, 2016; **91**: 368-377. DOI 10.1016/j.matdes.2015.11.117.

[2] Chatterjee S. and Pal T.K., *Wear*, 2003; **255**: 417-425. DOI 10.1016/S0043-1648 (03)00101-7.

[3] Mendez P.F., Barnes N., Bell K., Borle S.D., Gajapathi S.S., Guest S.D., Izadi H., Gol A.K. and Wood G., *J. Manuf. Process.*, 2014; **16**: 4-25. DOI 10.1016/j.jmapro. 2013.06.011.

[4] Kirchgaβner M., Badisch E. and Franek F., *Wear*, 2008; **265**: 772-779. DOI 10.1016/j.wear.2008.01.004.

[5] Yuksel N. and Sahin S., *Mater. Des.*, 2014; **58**: 491-498. DOI 10.1016/j.matdes. 2014.02.032.

[6] Chang C.M., Chen Y.C. and Wu W., *Tribol. Int.*, 2010*;* **43**: 929-934. DOI 10.1016/j.triboint.2009.12.045.

[7] Wang Y., Gou J., Chu R., Zhen D. and Liu S., *Tribol. Int.*, 2016; **103**: 102-112. DOI 10.1016/j.triboint.2016.06.041.

[8] Morsy M. and El-Kashif E., *Weld. World*, 2014; **58**: 491-497. DOI 10.1007/ s40194-014-0132-0.

[9] Zhang W., Zhong Z. and Kang S., *Int. J. Coal Sci. Technol.*, 2015; **2**: 254-260. DOI 10.1007/s40789-015-0082-1.

[10] Zahiri R., Sundaramoorthy R., Lysz P. and Subramanian C., *Surf. Coat. Technol.*, 2014; **260**: 220-229. DOI 10.1016/j. surfcoat.2014.08.076.

[11] Bendikiene R. and Kavaliauskiene L., *Weld. World*, 2017; **61**: 893-900. DOI 10.1007/s40194-017-0476-3.

[12] Buchely M.F., Gutierrez J.C., Leon L.M. and Toro A., *Wear*, 2005; **259**: 52-61. DOI 10.1016/j.wear.2005.03.002.

[13] Palani P.K. and Murugan N., *J. Mater. Process. Technol.*, 2007; **190**: 291-299. DOI 10.1016/j.jmatprotec.2007.02.035.

[14] Chandel R.S., Seow H.P. and Cheong F.L., *J. Mater. Process. Technol.*, 1997; **72**: 124-128. DOI 10.1016/S0924-0136(97) 00139-8.

[15] Gulenc B. and Kahraman N., *Mater. Des.*, 2003; **24**: 537-542. DOI 10.1016/S0261-3069(03)00082-7.

[16] Yamamoto S., *Arc Welding of Specific Steels and Cast Irons*, 3rd Edn., ShinkoWelding Service Co., Ltd., Japan, 2008.

[17] ASTM E384-11e1, *Standard Test Method for Knoop and Vickers Hardness of Materials*, ASTM International, West Conshohocken, PA, 2012, www.astm. org.

[18] ASTM G65-00e1, *Standard Test Method for Measuring Abrasion Using the Dry Sand/Rubber Wheel Apparatus*, ASTM International, West Conshohocken, PA, 2011, www.astm.org.

[19] Buchely M.F., Gutierrez J.C., Leon L.M. and Toro A., *Wear*, 2005 **259**: 52-61. DOI 10.1016/j.wear.2005.03.002.

[20] Carvalho M.C., Wang Y., Souza J.A.S., Braga E.M. and Li L., *Eng. Fail. Anal.*, 2016; **60**: 374-382. DOI 10.1016/j. engfailanal.2015.11.058.

[21] Gualco A., Svoboda H.G., Surian E.S. and de Vedia L.A., *Mater. Des.*, 2010; **31**: 4165-4173. DOI 10.1016/j.matdes.2010. 04.026.

[22] Lippold J.C. and Kotecki D.J., *Welding Metallurgy and Weldability of Stainless Steels*, 1st Edn., John Wiley & Sons, New Jersey, 2005.

[23] Wang X.L., Wang X.M., Shang C.J. and Misra R.D.K., *Mater. Sci. Eng. A*, 2016; **649**: 282-292. DOI 10.1016/j.msea.2015. 09.030.

[24] Yang J., Yang Y., Zhou Y., Qi X., Gao Y., Ren X. and Yang Q., *Weld. J.*, 2013; **92**: 225-230s.

[25] Tavares S.S.M., Pardal J.M., Da Silva M.R. and De Oliveira C.A.S., *Mater. Res.-Ibero-Am. J.*, 2014; **17**: 381-385. DOI 10.1590/S1516-14392013005000157.

[25] Avazkonandeh-Gharavol M.H., Haddad-Sabzevar M. and Haerian A., *J. Mater. Sci.*, 2009; **44**: 186-197. DOI 10.1007/s10853-008-3103-2.

[26] Coronado J.J., Caicedo H.F. and Gomez A.L., *Tribol. Int.*, 2009; **42**: 745-749. DOI 10.1016/j.triboint.2008.10.012.